Electronic Supplementary Material (ESI) for Journal of Materials Chemistry A.

Ultra-sensitive, flexible and transparent gas detection film based on well-ordered flat polypyrrole on single-layered graphene

Taeseung Yoon,[a†] Jaemoon Jun,[b†] Dong Yeon Kim,[c] Saeed Pourasad,[a] Tae Joo Shin,[d] Seong Uk Yu,[a] Wonjoo Na,[b] Jyongsik Jang,*[b] and Kwang S. Kim*[a]

[a.] Center for Superfunctional Materials, Department of Chemistry, [c.] Department of Chemical Engineering, [d.] UNIST Central Research Facilities (UCRF) and School of Natural Science, Ulsan National Institute of Science and Technology (UNIST), 50 UNIST-gil, Ulsan 44919, Republic of Korea

[b.]School of Chemical and Biological Engineering, College of Engineering, Seoul National University, 599 Gwanangno, Gwanakgu, Seoul 151-742, Republic of Korea

E-mail: kimks@unist.ac.kr (K.S.K.) or jsjang@plaza.snu.ac.kr (J.Jang)

Supplementary video

Movie S1. MD simulations representing formation steps of the flat conformation for 10C-PPy@SLG.

Movie S2. MD simulations representing formation steps of the tilted conformation for 70C-PPy@SLG.

Gas detection measurement. The measurement of changes in resistance was undertaken with a source meter connected to a computer at ambient temperature. Various analytes were introduced by mass flow controllers (MFC, SEC4400 from KNH, Dwyer Instrument, Inc.). The sensor devices were placed in a vacuum chamber within vapor inlet/outlet lines connected with MFC and an electrical feed-through connection. Real-time measurements were carried out with a constant current of 10^{-6} A (defined as $\Delta R/R_0 = (R-R_0)/R_0$, where R and R_0 are the real-time resistance and the initial resistance, respectively). After the sensor devices had been exposed to the target analyte for several minutes, the inert gas was introduced to the vacuum chamber to remove residual molecules that had become attached to the transducer. The response time was defined as the time required for the conductance to reach 90% of the saturation state after a target analyte was introduced, and the recovery time was defined as the time necessary for a sensor device to attain a conductance 10% above its original value in air.

Molecular Dynamics. NVT simulations were conducted using reactive force fields (ReaxFF)[S1,S2] in the LAMMPS package.[S3] The ReaxFF potential accounts for possible bond formation and dissociation of different bond orders, and contains van der Waals and Coulomb potentials for describing non-bond interactions between atoms. This potential calculates the charge polarization within the molecules, which is accessible using electronegativity equalization and charge equilibration (Q_{eq}) methods.[S4] A Nose/Hoover thermostat at room temperature was used for 0.5 and 1.0 ns for two flat layers and tilted PPy structure on SLG, respectively.

Density Functional Theory (DFT). Calculation of the binding energies of PPy@SLG with the gas molecules (NO_2 and NH_3) was performed with a generalized gradient approximation (GGA) functional, PBE[S5] using D3 dispersion correction scheme.[S6] The Vienna Ab-*initio* simulation

Package (VASP) was used.[S7,S8] The calculation was carried out on a 14.7 × 12.7 × 15.0 unit cell using a kinetic energy cutoff of 450 eV for the plane wave (PW) basis set, the projected augmented wave (PAW) pseudopotentials[S9,S10] and a Monkhorst-Pack grid of 3 × 3 × 1 k-points. In the charge transfer calculation between PPy and various gases, we used, for accuracy purposes, hybrid functional PBE0-D3[S11] with the 6-31G(d) basis set, and the NBO program[S12] in Gaussian09 was exploited for the NBO charge analysis.[S13]

Characterization. The surface morphologies were analyzed by atomic force microscopy (AFM, DI-3100, Veeco) and field-emission scanning electron microscopy (FE-SEM, Nova 230, FEI). Raman spectroscopy was carried out on a confocal Raman (Alpha 300R, WITec) with a laser wavelength of 532 nm. The chemical compositions of the samples were investigated by X-ray photoelectron spectroscopy (XPS, K-alpha, ThermoFisher) with a monochromated aluminum beam X-ray source. The electrochemical polymerizations were performed on an electrochemical workstation (VSP, Biologic). GIWAXD measurements were performed at the 6D UNIST-PAL beamline of the Pohang Accelerator Laboratory (PAL). The electrical measurements of sensors based on nC-PPy@SLG were conducted with a Keithley 2400-sourcemeter and a Wonatech WBCS 3000 potentiostat. Ultraviolet-visible (UV-Vis) transmittance spectra were characterized by a Lambda-35 spectrometer (Perkin-Elmer, USA).

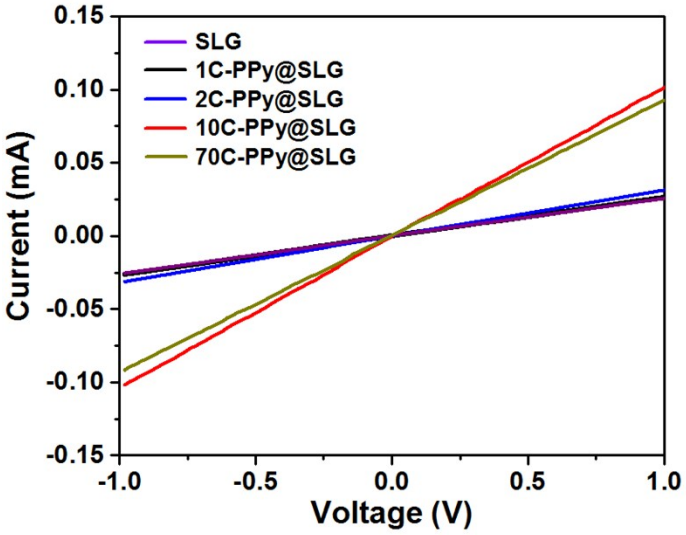

Figure S1. I–V characteristics of pristine SLG and nC-PPy@SLG at room temperature on the PET substrate. Current–voltage (I–V) curves of the pristine SLG and nC-PPy@SLG (n = 1, 2, 10, 70) were measured over voltage varying from -1.0 to 1.0 V. The linear modulations displayed in the I–V curves indicate excellent electrical contact, and the slope indicates the conductivity. The slope of the 10C-PPy@SLG is higher than those of other samples due to the well-ordered PPy orientation and crystallinity at PPy surface on the SLG.

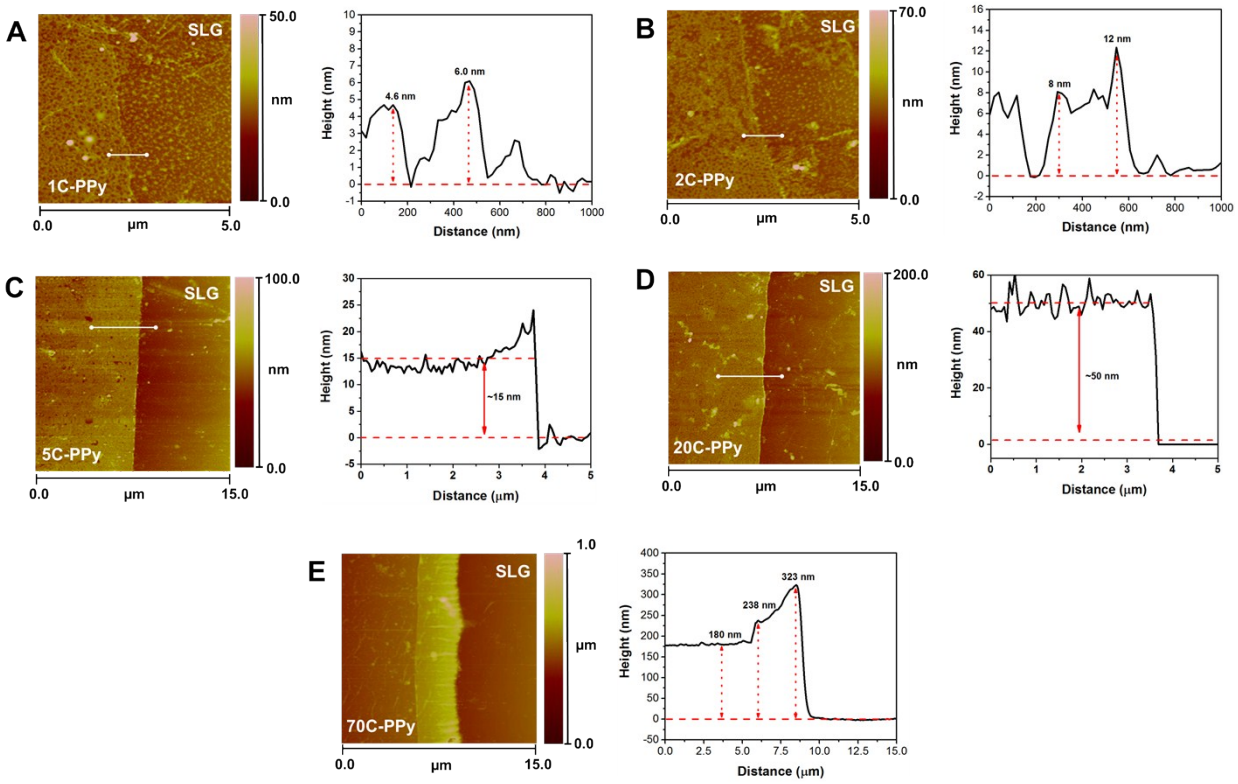

Figure S2. AFM images for height information. (A) 1C-PPy@SLG, (B) 2C-PPy@SLG, (C) 5C-PPy@SLG, (D) 20C-PPy@SLG, and (E) 70C-PPy@SLG. Because of differently repeated cyclic voltammetry (CV) for synthesizing PPy on SLG, the formed PPy exhibits different height and morphology. The 1C- to 20C-PPy@SLG are fitted with line profiling, whereas 70C-PPy@SLG is fitted with the overall area. The 1C-, 2C, and 5C-PPy@SLG show the branched-like morphology due to original PPy structure. The 20C-PPy@SLG shows similar morphology to 10C-PPy@SLG. However, 70C-PPy@SLG shows a uniform thick film as well as hill-like morphology near the contact of electric wire because the relatively low electron/hole mobility of PPy surface prevents PPy stacking.

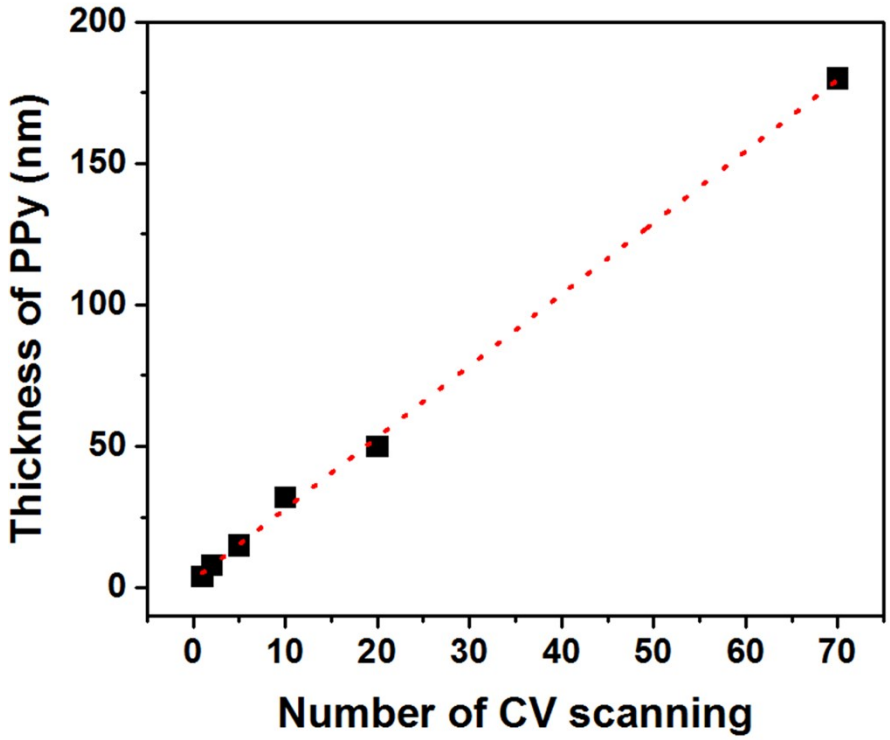

Figure S3. Graphs of PPy thickness against the number of CV scanning.

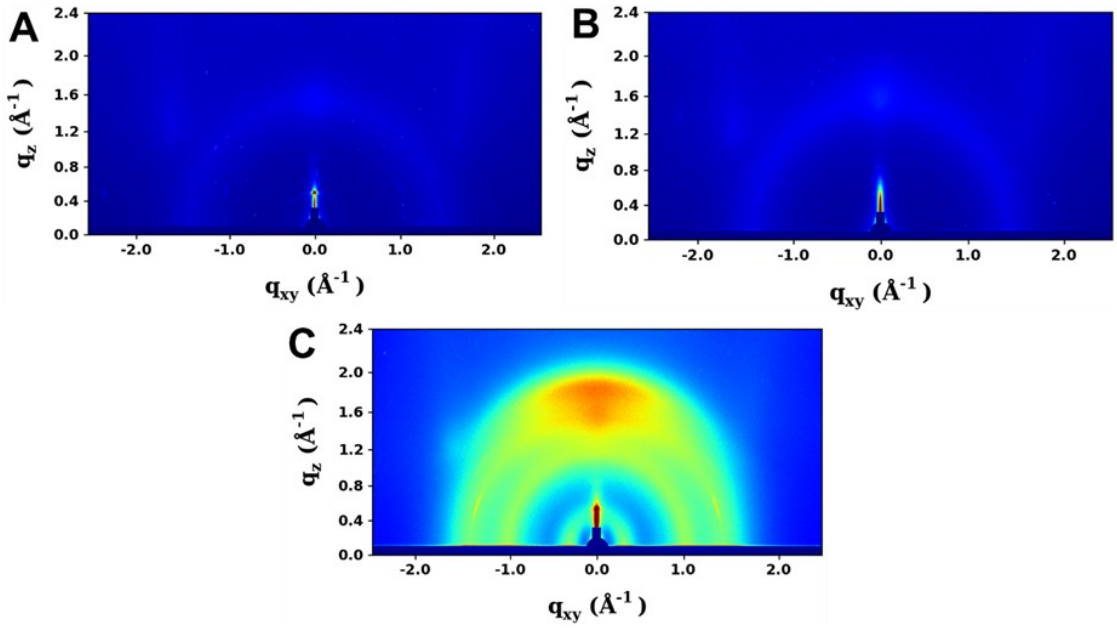

Figure S3. GIWAXD patterns. (A) 1C-PPy@SLG, (B) 2C-PPy@SLG, and (C) 70C-PPy@SLG.

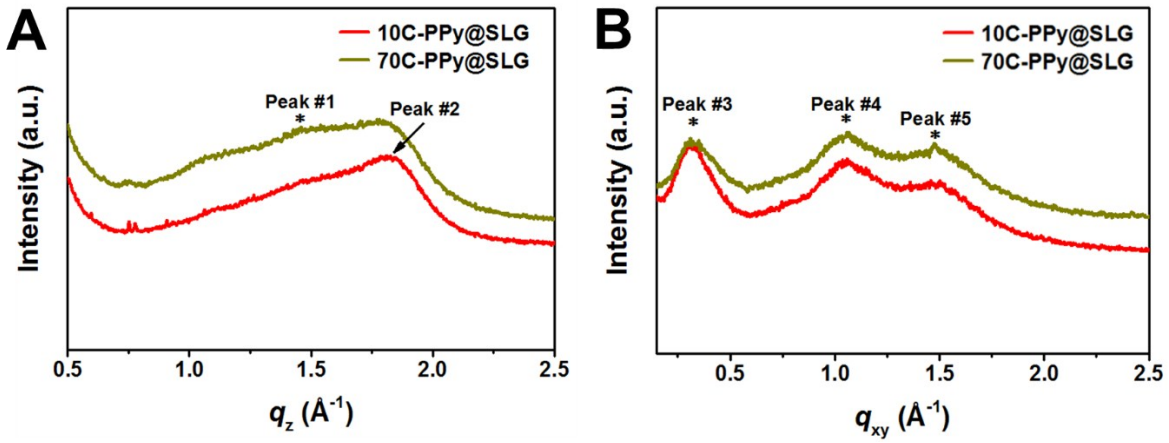

Figure S4. Linecuts derived from GIWAXD patterns. (A) Out-of-plane and (B) In-plane information. Profile plots of GIWAXD measurement were taken along the vertical and horizontal axes. At the out-of-plane linecuts, the peak #1 at q_z =1.486 Å^{-1} (d = 4.23 Å) and peak #2 at q_z = 1.847 Å^{-1} (d = 3.40 Å) were observed. At the in-plane linecuts, the peak #3 at q_{xy} = 0.3257 Å^{-1} (d = 19.29 Å), peak #4 at q_{xy} = 1.0815 Å^{-1} (d = 5.81 Å), and peak #5 at q_{xy} = 1.5054 Å^{-1} (d = 4.17 Å) are observed.

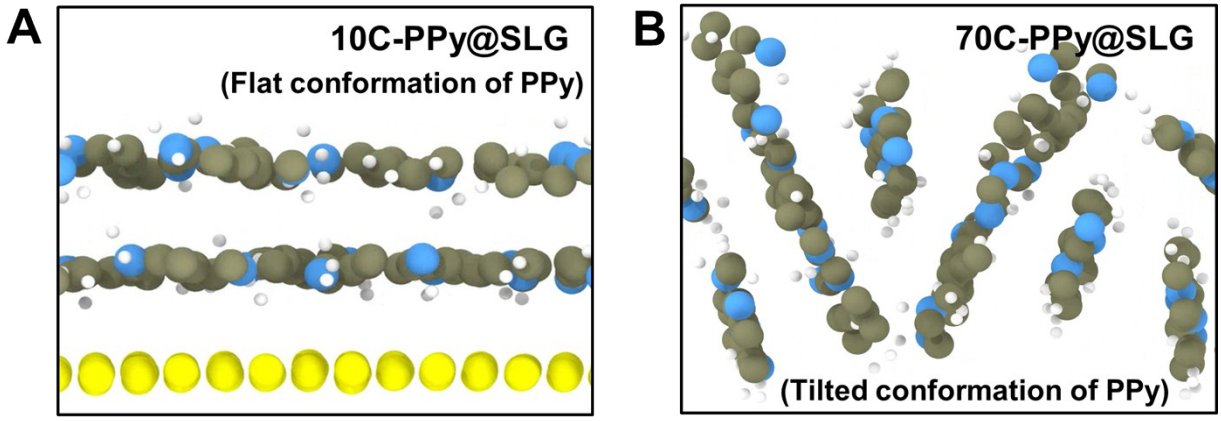

Figure S5. Schematic illustration for PPy conformation based on MD simulation (C: dark yellow, N: blue, H: white-gray, yellow atoms denote graphene). (A) Flat conformation of PPy for 10C-PPy@SLG. (B) Tilted conformation of PPy for 70C-PPy@SLG. The 10C-PPy@SLG shows flat PPy orientation due to strong π-stacking between SLG and PPy. However, the upper side of morphology for 70C-PPy@SLG shows tilted PPy orientation due to weak π-stacking between SLG and PPy.

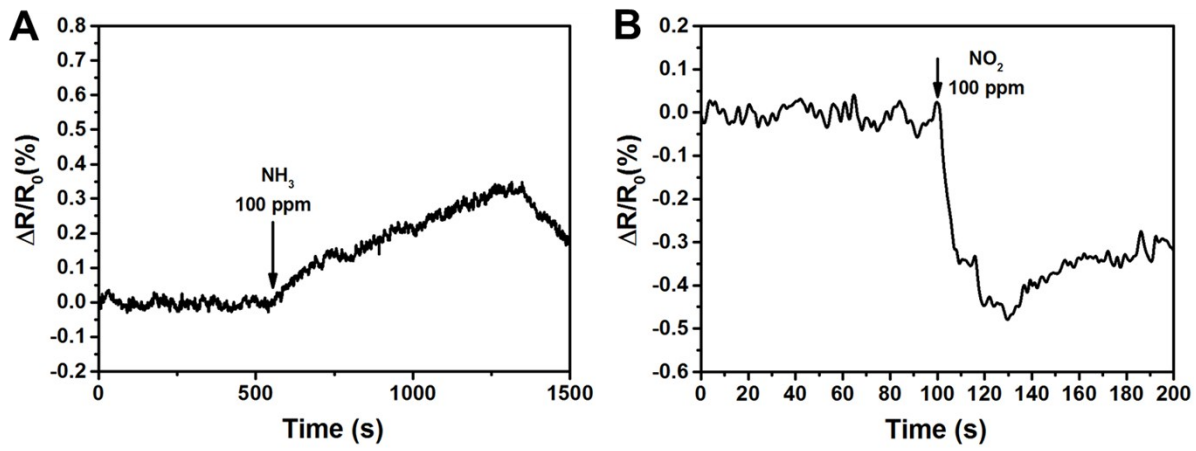

Figure S6. The minimum detectable level (MDL) for pristine SLG on the PET film upon the exposure to (A) 100 ppm NH_3 and (B) 100 ppm NO_2

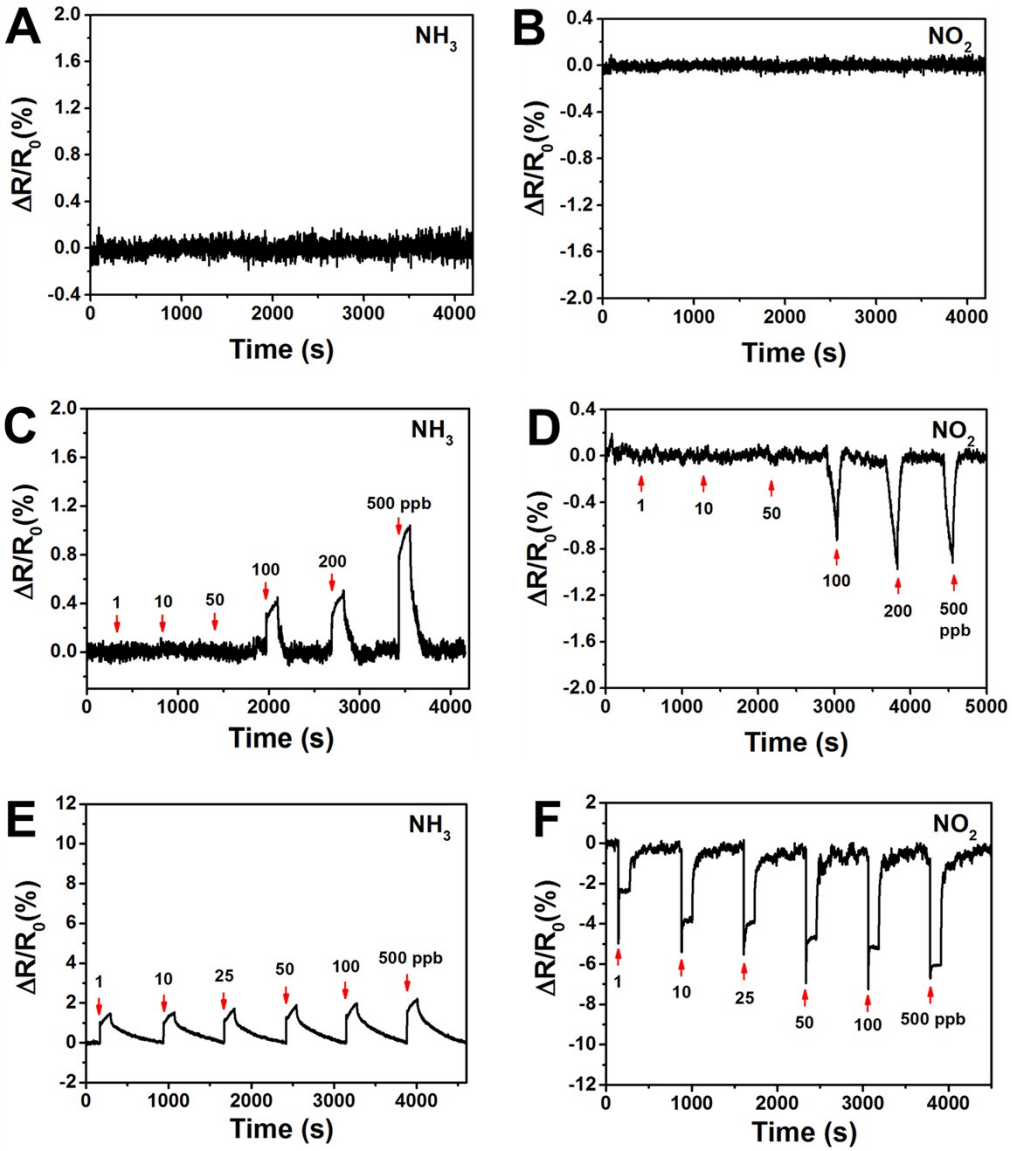

Figure S7. Gas sensor performances for 1C-, 2C-, and 70C-PPy@SLG. The 1C-PPy@SLG sensor does not work upon the exposure to (A) NH_3 and (B) NO_2 ranging from 0.1 to 500 ppb of concentration. The 2C-PPy@SLG sensor can detect concentrations above 100 ppb of (C) NH_3 and (D) NO_2. Their amorphous or weakly ordered PPy stuctures reduce the conductivity as well as detecting capacity. The 70C-PPy@SLG sensor shows very low detection limit for (E) NH_3 and (F) NO_2, however, sensitivity is relatively poor due to strong binding to PPy and analytes.

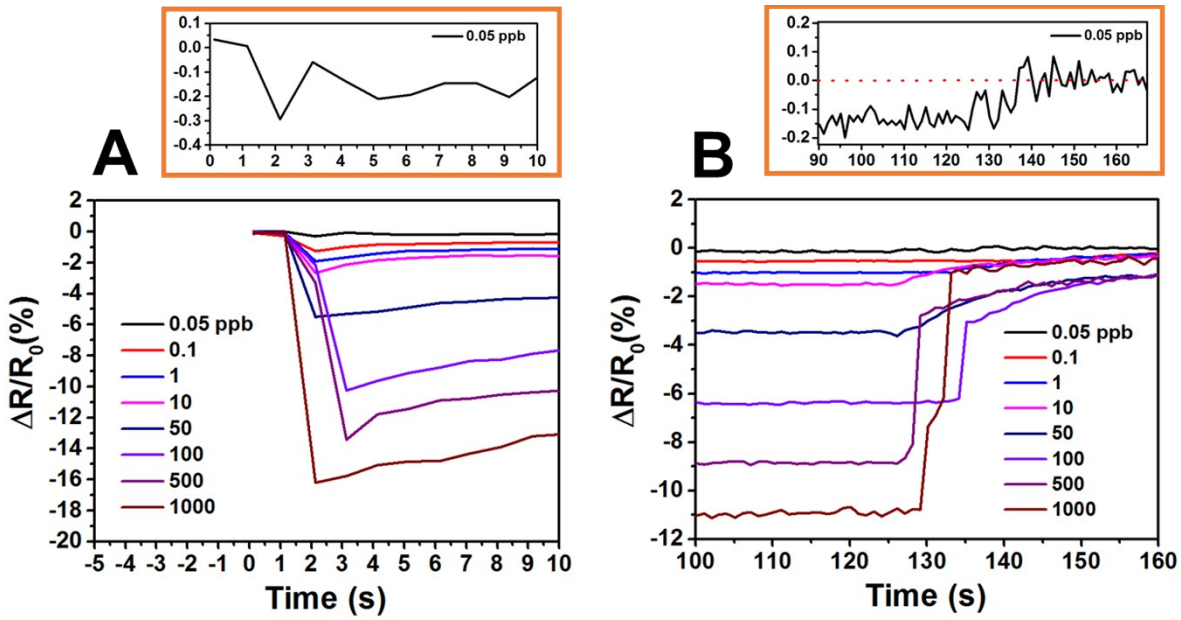

Figure S8. Response and recovery time upon exposure to various NO_2 gas concentrations for the 10C-PPy@SLG sensor. (A) Response and (B) recovery signal information. The graphs in orange boxes show enlarged data for 0.05 ppb.

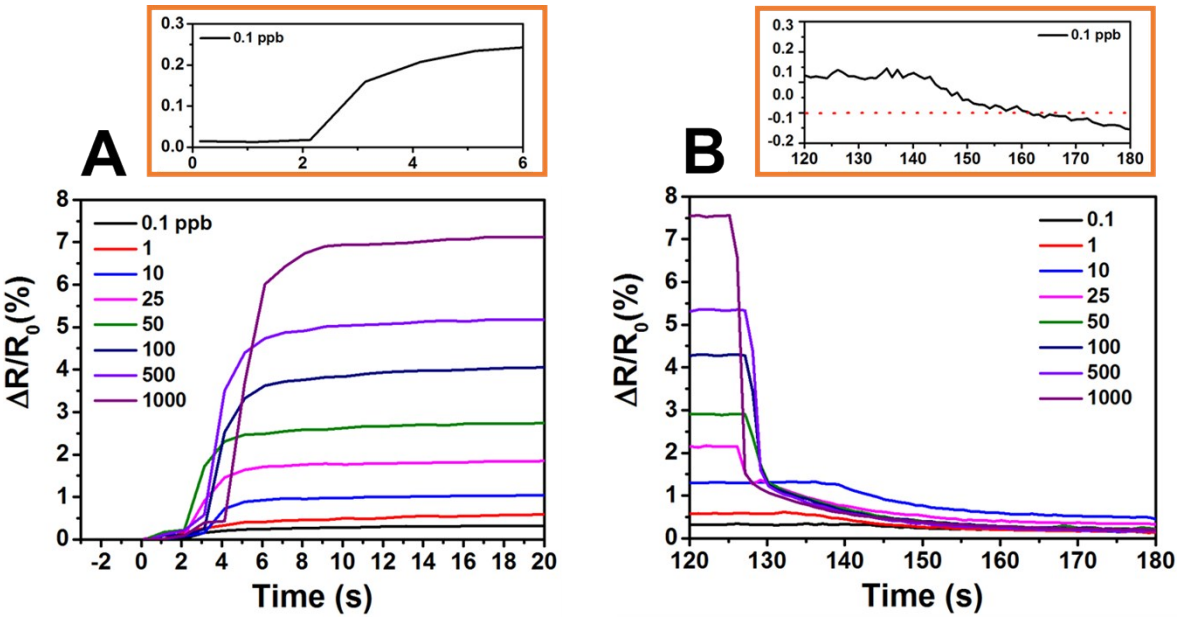

Figure S9. Response and recovery time upon exposure to various NH_3 gas concentrations for the 10C-PPy@SLG sensor. (A) Response and (B) recovery signal information. The graphs in orange boxes show enlarged data for 0.1 ppb.

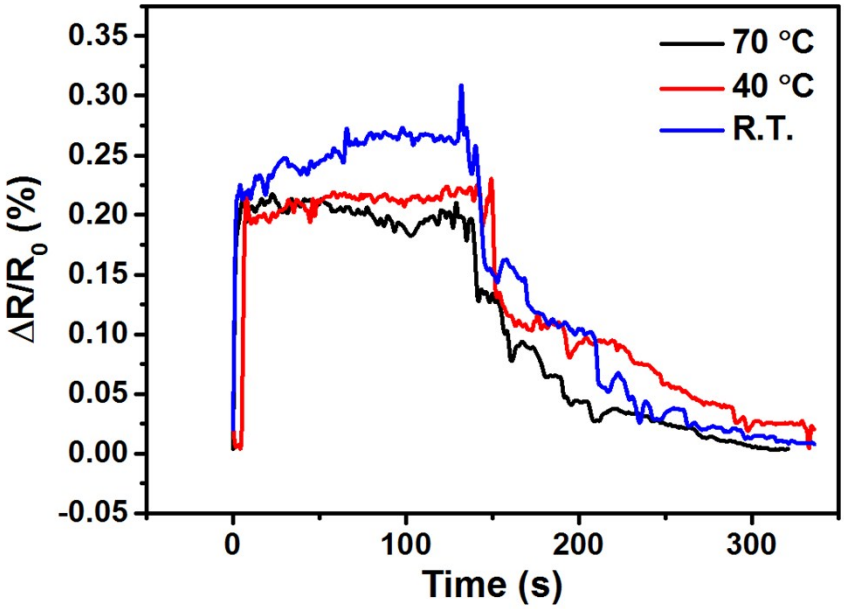

Figure S10. Dynamic properties of the 10C-PPy@SLG sensor. The responses and recoveries time at various temperatures upon exposure to 0.1 ppb of NH_3 gas.

NO_2	NH_3	Acetone	H_2O	Benzene
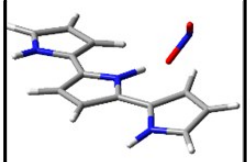		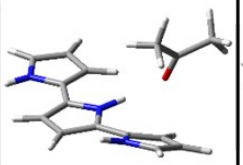		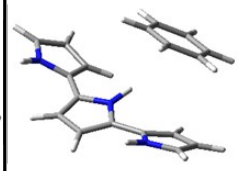
Q_{nbo}: -0.744	Q_{nbo}: 0.052	Q_{nbo}: 0.039	Q_{nbo}: 0.026	Q_{nbo}: 0.004
Toluene	**Ethanol**	**Naphthalene**	**Chloroform**	**Methanol**
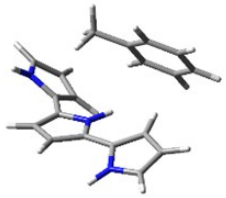	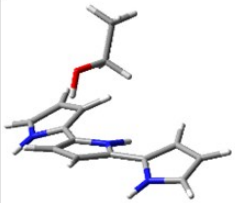	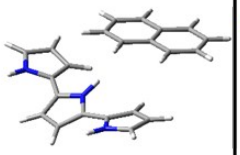	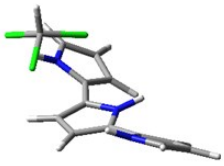	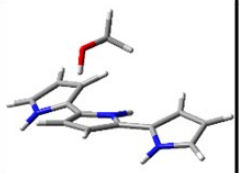
Q_{nbo}: 0.003	Q_{nbo}: -0.010	Q_{nbo}: 0.003	Q_{nbo}: 0.004	Q_{nbo}: -0.010

Figure S11. Charge transfer (Q_{nbo}) at the optimized structures of pyrrole and various guest molecules. The calculation were carried out at the PBE0-D3/6-31G(d) level of theory. Certain conformations, even though larger binding energies, were not considered in this charge transfer calculation because such structures are not suitable as the PPy is stacked on another PPy and surrournded by neighboring PPy molecules in the **10C-PPy@SLG** sensor.

Table S1. Sensor properties for the detection of NO_2 and NH_3. The performances of 1C, 2C, 10C, and 70C-PPy@SLG are summarized.

Sensing material	Analytes	Detection limit	Response time (upon exposure to gas concentration)	Recovery time (upon exposure to gas concentration)
1C-PPy@SLG	NH_3 NO_2	–	–	–
2C-PPy@SLG	NH_3 NO_2	100 ppb 100 ppb	7 s (100 ppb) 19 s (100 ppb)	17 s (100 ppb) 12 s (100 ppb)
10C-PPy@SLG	**NH_3** **NO_2**	**0.04 ppb** **0.03 ppb**	**1 s (0.1 ppb)** **2 s (0.05 ppb)**	**10 s (0.1 ppb)** **7 s (0.05 ppb)**
70C-PPy@SLG	NH_3 NO_2	1 ppb 1 ppb	3 s (1 ppb) 5 s (1 ppb)	40 s (1 ppb) 21 s (1 ppb)

Table S2. Response and recovery time of the 10C-PPy@SLG sensor upon exposure to NO_2 and NH_3 gas. The response time was defined as the time required for the conductance to reach 90% of the saturation state after a target analyte was introduced, and recovery time was defined as the time necessary for a sensor devices to attain a conductance 10% above its original value in air.

Analyte	NO_2		NH_3	
Gas concentration (ppb)	Response time (s)	Recovery time (s)	Response time (s)	Recovery time (s)
0.05	2	7	–	–
0.1	4	8	1	10
1	6	15	3	27
10	6	18	3	37
25	6	20	5	41
50	5	21	5	45
100	6	23	6	45
500	6	42	15	61
1000	11	69	32	62

References

S1 A. C. Van Duin, S. Dasgupta, F. Lorant and W. A. Goddard, *J. Phys. Chem. A,* 2001, **105**, 9396-9409.

S2 T. P. Senftle, S. Hong, M. M. Islam, S. B. Kylasa, Y. Zheng, Y. K. Shin, C. Junkermeier, R. Engel-Herbert, M. J. Janik, H. M. Aktulga, T. Verstraelen, A. Grama and A. C. T. van Duin, *npj Comput. Mater.,* 2016, **2**, 15011.

S3 S. Plimpton, *J. comput. Phys.,* 1995, **117**, 1-19.

S4 A. K. Rappe and W. A. Goddard III, *J. Phys. Chem.* 1991, **95**, 3358-3363.

S5 J. P. Perdew, K. Burke and M. Ernzerhof, *Phys. Rev. lett.,* 1996, **77**, 3865.

S6 S. Grimme, J. Antony, S. Ehrlich and H. Krieg, *J. Chem. Phys.,* 2010, **132**, 154104.

S7 G. Kresse and J. Hafner, *Phys. Rev. B,* 1993, **47**, 558-561.

S8 G. Kresse and J. Furthmüller, *Phys. Rev. B,* 1996, **54**, 11169.

S9 P. E. Blöchl, *Phys. Rev. B,* 1994, **50**, 17953-17979.

S10 G. Kresse and D. Joubert, *Phys. Rev. B,* 1999, **59**, 1758.

S11 C. Adamo and V. Barone, *J. Chem. Phys.* 1999, **110**, 6158-6170.

S12 F. Weinhold and C. R. Landis, *Chem. Educ. Res. Pract.,* 2001, **2**, 91-104.

S13 M. J. Frisch, G. W. Trucks, H. B. Schlegel, G. E. Scuseria, M. A. Robb, J. R. Cheeseman, G. Scalmani, V. Barone, B. Mennucci, G. A. Petersson, H. Nakatsuji, M. Caricato, X. Li, H. P. Hratchian, A. F. Izmaylov, J. Bloino, G. Zheng, J. L. Sonnenberg, M. Hada, M. Ehara, K. Toyota, R. Fukuda, J. Hasegawa, M. Ishida, T. Nakajima, Y. Honda, O. Kitao, H. Nakai, T. Vreven, J. A. Montgomery Jr., J. E. Peralta, F. Ogliaro, M. Bearpark, J. J. Heyd, E. Brothers, K. N. Kudin, V. N. Staroverov, R. Kobayashi, J. Normand, K. Raghavachari, A. Rendell, J. C. Burant, S. S. Iyengar, J. Tomasi, M. Cossi, N. Rega, J. M. Millam, M. Klene, J. E. Knox, J. B. Cross, V. Bakken, C. Adamo, J. Jaramillo, R. Gomperts, R. E. Stratmann, O. Yazyev, A. J. Austin, R. Cammi, C. Pomelli, J. W. Ochterski, R. L. Martin, K. Morokuma, V. G. Zakrzewski, G. A. Voth, P. Salvador, J. J. Dannenberg, S. Dapprich, A. D. Daniels, Ö. Farkas, J. B. Foresman, J. V. Ortiz, J. Cioslowski and D. J. Fox, Gaussian 09, Revision B.01, Wallingford CT, 2009.